Incoherent white-light solitons in nonlinear periodic lattices

Pezer, Robert; Buljan, Hrvoje; Bartal, Guy; Segev, Mordechai; Fleischer, Jason W.

Incoherent white-light solitons in nonlinear periodic lattices

R. Pezer and H. Buljan
Department of Physics, University of Zagreb, Bijenička c. 32, 10000 Zagreb, Croatia

G. Bartal and M. Segev
Physics Department, Technion - Israel Institute of Technology, Haifa 32000, Israel

J. W. Fleischer
Electrical Engineering Department, Princeton University, New Jersey 08544, USA
(Received 9 January 2006; published 18 May 2006)

We predict the existence of lattice solitons made of incoherent white light: lattice solitons made of light originating from an ordinary incandescent light bulb. We find that the intensity structure and spatial power spectra associated with different temporal frequency constituents of incoherent white-light lattice solitons (IWLLSs) arrange themselves in a characteristic fashion, with the intensity structure more localized at higher frequencies, and the spatial power spectrum more localized at lower frequencies; the spatial correlation distance is larger at lower frequency constituents of IWLLSs. This characteristic shape of incoherent white-light lattice solitons reflects the fact that diffraction is stronger for lower temporal frequency constituents, while higher frequencies experience stronger effective nonlinearity and deeper lattice structure.

DOI: 10.1103/PhysRevE.73.056608 PACS number(s): 42.65.Tg

I. INTRODUCTION

The behavior of partially coherent light in nonlinear photonic lattices depends on the threefold interplay between the nonlinearity, the lattice properties, and the coherence properties of the light. This direction of research is motivated by the following facts: (i) the behavior of light in periodic systems is driven by interference, which crucially depends on the coherence of the light, and (ii) most of the light sources encountered in nature (e.g., the Sun) emit partially coherent light. Partial coherence of light becomes important when the coherence length scale(s) become comparable with the characteristic length scales of the periodic system, e.g., the lattice spacing. Several studies have addressed this direction of research recently, starting with the prediction [1] and the observation [2] of random-phase (incoherent) lattice solitons (RPLSs), and the development of an experimental technique for Brillouin-zone spectroscopy of nonlinear photonic lattices [3]. Following the experimental findings of Ref. [2], a subsequent theoretical study of the evolution of a simple incoherent beam into a RPLS [4] was carried out. Later on, random-phase gap-lattice solitons, arising from the Bloch modes associated with the anomalous diffraction regions, were studied in one-dimensional [(1+1)D] nonlinear waveguide arrays, under nonlinear self-defocusing conditions [5,6]. Such gap RPLSs were demonstrated experimentally and studied theoretically very recently, in a (2+1)D geometry [7].

The interest in the dynamics of partially incoherent light beams in nonlinear photonic lattices stems from two directions of research that have attracted considerable attention over the past decade. The first one is the area of lattice solitons (often called "discrete solitons"). In optics, these entities were mostly studied through propagation of coherent light beams in nonlinear photonic lattices [8–23]. The second is the area of incoherent solitons and related nonlinear phenomena such as modulation instability (MI) [24–42]. These phenomena were studied through the propagation dynamics of incoherent light beams in noninstantaneous nonlinear homogeneous media [24–35,37–40].

Let us now briefly address the background in both areas. The first area has started with the 1988 prediction of coherent optical solitons in nonlinear arrays of coupled waveguides [10], which were observed ten years later [12]. The dynamics of coherent light in linear and nonlinear periodic lattices was subsequently addressed in many studies, to name a few (e.g., see Refs. [8,9] and references therein): the observations of Bloch oscillations [13], diffraction management [14], studies of gap solitons [11,16], multiband solitons [18,19], higher-band Floquet-Bloch solitons [20], soliton trains [21], and modulational instability in nonlinear waveguide arrays [22]. Important progress has been made recently with the optical induction technique [15,17], which is used to construct (2+1)D nonlinear waveguide arrays. This system was utilized for the first observation of (2+1)D lattice solitons in any two-dimensional periodic system in nature [17].

The second area started with the 1996 experimental observation of incoherent solitons [25], which was carried out in a homogeneous nonlinear medium with a noninstantaneous response. This was followed by a number of experiments (e.g., see Ref. [24] and references therein) in several types of nonlinear media (e.g., photorefractives [25], liquid crystals [35], etc.). Several theoretical approaches were used to describe the evolution of incoherent light in noninstantaneous nonlinear media. The frequently used theories are the coherent density theory [27], the modal theory [28], and the mutual coherence theory [29], which are formally equivalent [30]. Other theories include the geometric optics approach (applicable in the ray-optics limit) [31], and the statistical physics approach based on the Wigner transform [32]. The discovery of incoherent solitons raised fundamental ques-

tions about the existence of the closely related phenomenon of modulation instability with incoherent light. Following this motivation, theoretical and experimental studies have demonstrated that incoherent modulation instability indeed occurs, but only if the nonlinearity exceeds a specific threshold value, which in turn is determined by the coherence properties of the light [33,34]. In their original concept [24–26], incoherent solitons were studied with a noninstantaneous nonlinearity, with a response time of the nonlinearity much longer than the characteristic time of random fluctuations of the optical field. However, it has been pointed out that other mechanisms [36,42] may provide support for incoherent solitons in instantaneous media as well.

The incoherent light source that was used in the first experiment on incoherent solitons [25] was a laser beam sent through the rotating diffuser, that is, the light was spatially incoherent but quasi-monochromatic. The next experiment [26] went further and used an ordinary incandescent light bulb as a light source; such light is both spatially and temporally incoherent (incoherent white light). Theoretically, several characteristic features of incoherent white-light solitons [37] and modulation instability [38,39] of such light in noninstantaneous nonlinear media were subsequently studied. In such a system, the evolution of a broad band of frequencies is coupled with the nonlinearity giving rise to interesting features such as collective threshold for the onset of MI [38,39] and many others. More recently, incoherent white light solitons were studies in nonlocal media as well [41].

Here we study the properties of incoherent white-light lattice solitons (IWLLSs) in (1+1)D nonlinear waveguide arrays with a noninstantaneous nonlinearity. The motivation for this study is twofold. First, the propagation of nonmonochromatic light in periodic structures is inherently interesting, because even in the linear case, each frequency constituent behaves differently in the lattice (e.g., the Bragg angle depends on the wavelength). Second, when the lattice is nonlinear, the various components of the temporal spectrum are coupled in their propagation dynamics. Such physical setup is feasible experimentally and is expected to yield interesting phenomena. For concreteness, we analyze here IWLLSs originating from the light source used in Ref. [26], which spans the visible range from $\lambda = 400-700$ nm, and is both spatially and temporally incoherent.

We emphasize that these solitons are inherently statistical in nature, with an optical field structure that varies randomly in time. Therefore, they physically differ from e.g., Manakov-type vector lattice solitons [18,19], or the more recently studied polychromatic multigap solitons [23]. For example, the latter solitons involve the coupled evolution of spatially coherent beams at several different wavelengths; by contrast, the incoherent white light solitons studied here possess a broad continuum of frequency components, and are both spatially and temporally incoherent.

In this paper, we self-consistently calculate the properties of a typical IWLLS solution. We identify the behavior of each temporal frequency constituent of such an IWLLS, finding the intensity profile and coherence properties at each frequency ω. We find that these features, at each frequency, are affected by the lattice in a fashion similar to that of a quasimonochromatic random-phase lattice soliton. However, the intensity structure is more localized at higher frequencies (violet side of the spectrum) than at lower frequencies. The opposite holds for the spatial power spectrum that is more localized at lower frequencies (red side of the spectrum). This characteristic shape of IWLLSs reflects the fact that diffraction is stronger for lower temporal frequency constituents, while higher frequencies experience stronger effective nonlinearity and deeper lattice structure. Finally it is shown that IWLLSs are experimentally accessible, as the dynamics in a nonlinear waveguide array can (under proper nonlinear conditions) naturally evolve from a "simple" (bell-shaped) incoherent white-light input beam into an IWLLS. The input beam acquires the properties of an IWLLS during propagation, in a fashion similar to the nonlinear reshaping process of a spatially incoherent quasimonochromatic beam (see Refs. [2,4,6] for examples of such dynamics).

II. DESCRIPTION OF THE PHYSICAL SYSTEM

The physical system is as follows. The light source (continuously) emits spatially and temporally incoherent light (e.g., an incandesent light bulb generates such light [26]), with a broad temporal power spectrum ($\lambda = 400-700$ nm). A beam of such light is incident upon a (1+1)D nonlinear waveguide array with noninstantaneous nonlinearity. This is the key physical property of our system: the nonlinearity cannot follow the fast fluctuations of the randomly fluctuating field but rather responds to the total time-averaged light intensity (integrated over all frequencies) [26,37–39]. This allows the creation of a smooth self-induced defect in the lattice that enables the self-guidance of all the spectral components of the incoherent beam.

The state of the system can be described by using the mutual coherence function in the space-frequency domain, where the intensity structure and spatial coherence properties at a given frequency ω are described by the mutual spectral density $B_\omega(x_1, x_2, z)$ [37,38]; here x is the spatial coordinate while z denotes the propagation axis coordinate. The intensity structure at the temporal frequency constituent ω is contained within the diagonal of the mutual spectral density $I_\omega(x,z) = B_\omega(x,x,z)$. The information on the spatial coherence properties at frequency ω is extracted by normalizing $B_\omega(x_1, x_2, z)$

$$\mu_\omega(x_1,x_2,z) = B_\omega(x_1,x_2,z)/\sqrt{B_\omega(x_1,x_1,z)B_\omega(x_2,x_2,z)}. \quad (1)$$

The quantity $\mu_\omega(x_1, x_2, z)$ is referred to as the complex coherence factor at frequency ω. It expresses the spatial correlation properties of the randomly fluctuating optical field. Hence, the spatial correlation distance at frequency ω is related to the characteristic width of $\mu_\omega(x_1, x_2, z)$. The total time-averaged intensity is obtained by integrating $B_\omega(x,x,z)$ over all temporal frequencies $I_{\mathrm{tot}}(x,z) = \int d\omega B_\omega(x,x,z)$.

Within the modal theory [28,37], the mutual spectral density $B_\omega(x_1, x_2, z)$ is expressed in terms of modes $\psi_{\omega;m}(x,z)$ and their modal weights $d_{\omega;m}$

$$B_\omega(x_1,x_2,z)=\sum_m d_{\omega;m}\psi^*_{\omega;m}(x_2,z)\psi_{\omega;m}(x_1,z). \quad (2)$$

The evolution of modes $\psi_{\omega;m}$, and hence the evolution of the correlation function $B_\omega(x_1,x_2,z)$, along the z axis, is governed by a set of integrodifferential equations [37,38]

$$i\frac{\partial\psi_{\omega;m}}{\partial z}+\frac{1}{2k_\omega}\frac{\partial^2\psi_{\omega;m}}{\partial x^2}+\frac{k_\omega}{n_0}V(x,z)\psi_{\omega;m}(x,z)=0, \quad (3)$$

where the potential $V(x,z)=p(x)+\delta n(I_{\rm tot})$ is made up of the linear $p(x)=p(x+D)$, and the nonlinear term $\delta n(I_{\rm tot})$, where $I_{\rm tot}=\int d\omega I_\omega(x,z)$, while $I_\omega(x,z)=\Sigma_m d_{\omega;m}|\psi_{\omega;m}(x,z)|^2$ denotes the intensity structure at frequency ω. In this paper we consider self-focusing media $\partial\delta n(I)/\partial I>0$, however, from our discussion it follows that the qualitative features of IWLLSs discussed below should hold for IWLLSs in self-defocusing media as well, with the distincion of their Floquet-Bloch power spectra being located mostly in the anomalous diffraction regions of the momentum space, as has been discussed for quasimonochromatic spatially incoherent solitons (e.g., see [4]). In order to extract the behavior of the intensity structure, coherence, and spatial spectra at a given temporal frequency ω in the most simple fashion, we assume that the medium is dispersionless and the photosensitivity is frequency independent. That is, the linear and the nonlinear contributions to the index of refraction are frequency independent; see Refs. [37,39] for discussion. We also neglect the possible strong intensity fluctuations of the source; such an effect can be included in Eq. (3) by using an effective nonlinear term [40].

Solitons occur in our system when diffraction of a spatially localized, incoherent white-light beam, is exactly balanced by the nonlinear self-focusing (or self-defocusing). This is far more involved than in the monochromatic case since an exact balance has to happen for every color constituent simultaneously. The self-consistency principle for an IWLLS is as follows: An incoherent white-light beam induces a defect in the periodic lattice, which has localized defect states. Because the coefficients in Eq. (3) are frequency dependent ($k_\omega=n_0\omega/c$), the defect modes, and their propagation constants (which are located in the gaps of the spectrum of the linear system) differ for each frequency component. If all the modes $\psi_{\omega;m}$ of each frequency constituent making up the incoherent beam coincide with the defect modes at corresponding frequencies, then the self-consistency loop is closed, and the incoherent white-light beam self-traps in the lattice, forming an IWLLS. Mathematically, this means that

$$\psi_{\omega;m}(x,z)=u_{\omega;m}(x)e^{i\kappa_{\omega;m}z},$$

where $u_{\omega;m}(x)$ are orthonormal (real) eigenfunctions, and $\kappa_{\omega;m}$ real eigenvalues of the defect modes at the frequency ω, obtained self-consistently from the eigenvalue equation

$$\frac{1}{2k_\omega}\frac{d^2u_{\omega;m}}{dx^2}+\frac{k_\omega}{n_0}V(x)u_{\omega;m}=\kappa_{\omega;m}u_{\omega;m}(x), \quad (4)$$

where

$$V(x)=p(x)+\delta n\left(\int d\omega\sum_m d_{m;\omega}|u_{m;\omega}(x)|^2\right).$$

The eigenvalues of the localized defect modes $\kappa_{\omega;m}$ are located in the gaps of the spectrum of the linear system (including the semi-infinite gap above the first band). We emphasize that the band-gap structure of the linear system differs for each frequency component, as shown below.

III. INTENSITY STRUCTURE, SPATIAL POWER SPECTRA, AND COHERENCE

In this section we present an example of an IWLLS in a saturable self-focusing medium $\delta n(I)=\gamma I/(1+I/I_S)$, and analyze its intensity structure, spatial power spectra (see the Appendix for definitions), and coherence properties at each frequency ω. We have already noted that the coefficients in the evolution Eq. (3) are frequency dependent, e.g., the (free-space) diffraction term, $\propto k_\omega^{-1}\partial^2/\partial x^2$, is stronger at lower frequencies. From this it follows that the IWLLS structure should differ for different frequency constituents. In order to analyze this, it is convenient to rewrite Eq. (4) in dimensionless units

$$\frac{d^2u_{\omega;m}}{d\xi^2}+V_{\rm eff}(\omega;\xi)u_{\omega;m}=\kappa_m^{\rm eff}(\omega)u_{\omega;m}(\xi), \quad (5)$$

where $\xi=x/x_0$, x_0 is a spatial length scale, $\kappa_m^{\rm eff}(\omega)=2k_\omega x_0^2\kappa_{\omega;m}$ is *the effective propagation constant*, while

$$V_{\rm eff}(\omega;\xi)=\frac{2(k_\omega x_0)^2}{n_0}\{p(\xi)+\delta n(I_{\rm tot})\} \quad (6)$$

is *the effective potential* felt by each frequency component ω.

We would like now to examine each frequency constituent of the IWLLS individually, and extract its features that arise solely from the fact that the effective potential is frequency dependent. To do that, it is convenient to analyze solutions for which the temporal power spectrum is uniform. (Otherwise, if one of the frequencies would strongly dominate within the temporal power spectrum, it would "guide" the other frequencies, and the nonlinear features discussed below would be harder to distinguish).

The parameters of the nonlinearity and the lattice used in the calculations are $\gamma I_S=1.5\cdot10^{-4}$, the periodic potential term is $p(x)=p_0\Sigma_j\{\exp(-[(x-jD)/x_c]^8\}$, where $x_c=3.7$ μm, $D=10$ μm, and $p_0=4.5\cdot10^{-4}$, while the spatial length-scale $x_0=2$ μm. The linear part of the index of refraction is $n_0=2.3$ [as for the Strontium-Barium-Niobate (SBN) crystals used in such experiments]. The light source spans the entire visible range $\lambda=400-700$ nm, which determines the span of $k_\omega=n_0\omega/c=2\pi n_0/\lambda$ (frequency components span from $2.69-4.71\times10^{15}$ Hz). With these parameters, the IWLLSs are calculated self-consistently from Eq. (4) by using the numerical procedure described in [18]. In order to extract the main frequency-dependent features of the IWLLS, we chose the same modal structure for each frequency component. The power distribution within the populated localized modes aris-

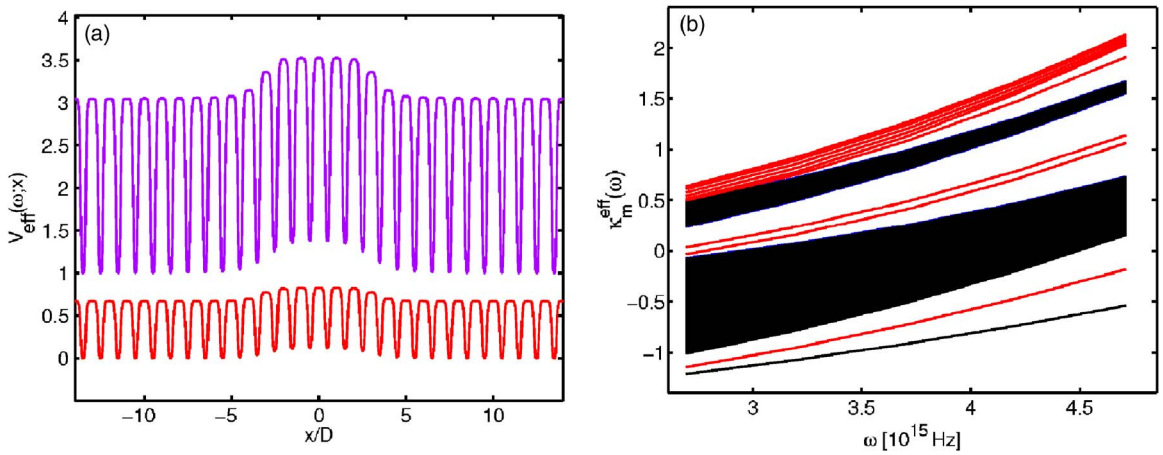

FIG. 1. (Color online) The effective potentials and band gap structure at different temporal frequencies. (a) The effective potential $V_{\text{eff}}(\omega;x)$ for $\lambda=400$ nm (violet line) and $\lambda=700$ nm (red line) of the self-consistently calculated IWLLS (the potential value for the violet light is shifted upwards by 1 for better comparison). (b) The band gap structure of the lattice (shaded regions denote bands), and the effective propagation constants $\kappa_m^{\text{eff}}(\omega)$ of the populated soliton modes (red lines).

ing from the Bloch modes of the linear bands (at each temporal frequency) is as follows:

(i) First band (total 72%) six modes: 17.8, 16.2, 13.7, 10.8, 8.0, and 5.5 %

(ii) Second band (total 25%) two modes: 18.0 and 7.0 %,

(iii) Third band (total 3%) one mode: 3.0%.

The total power within the soliton is 11 I_0x_0. Figure 1 illustrates the effective potential, the effective band-gap structure of the lattice, and the propagation constants of the soliton. We observe two important features: First, the effective band-gap structure (the linear lattice properties) of the various frequency components differ from one another. The gaps are wider and the bands are narrower at higher frequencies. This follows from the fact that the effective lattice depth increases with the increase of frequency [see Eq. (6)]. Second, the effective nonlinear index change is larger at higher frequencies. The effective propagation constants $\kappa_m^{\text{eff}}(\omega)$ are pushed deeper into the gaps for higher frequencies; this is consistent with the deeper effective lattice and stronger effective nonlinearity "felt" by the higher frequencies. It should be stated

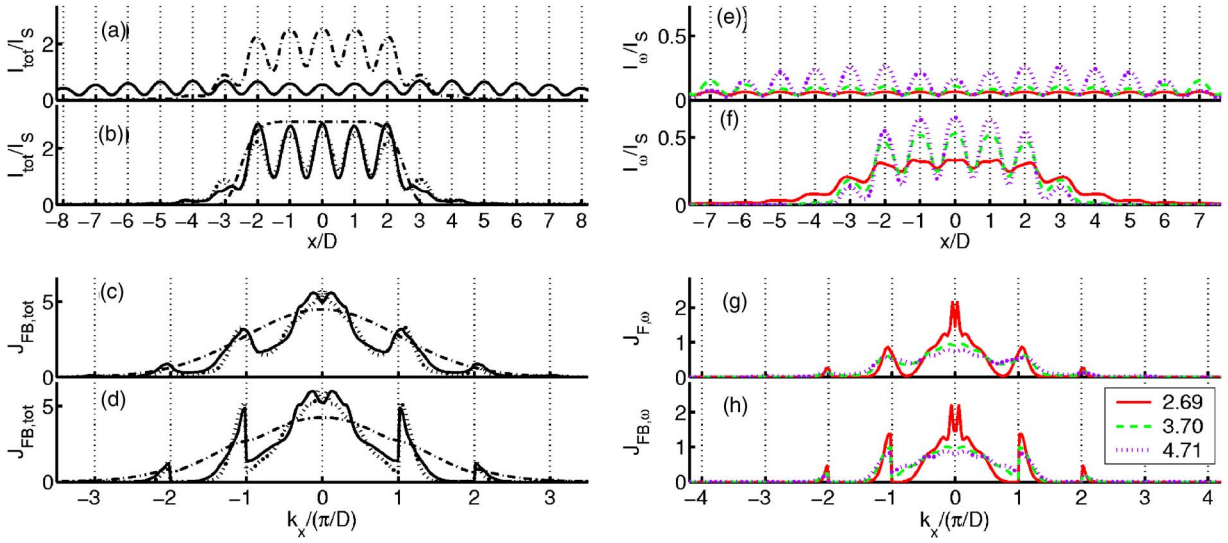

FIG. 2. (Color online) Intensity profile and spatial power spectra of the IWLLS example in a nonlinear waveguide array displaying a self-focusing nonlinearity. Left column: soliton quantities integrated over all frequency constituents. (a) Intensity profile of the IWLLS (dot-dashed line), and broadened intensity profile of the IWLLS input beam after linear diffraction for 42 mm (solid line) in a linear lattice. (b) Intensity structure of the self-consistently calculated IWLLS (solid line), the experimentally accessible (simple) input beam (dot-dashed line), and the structure of the simple input beam after evolution for 42 mm (dotted line) under the nonlinear conditions that support the self-consistently calculated IWLLS. (c) Same as (b) for the Fourier power spectrum, and (d) same as (b) for the Floquet-Bloch power spectrum (the spectra are in arbitrary units). Right column: soliton quantities of different wavelength constituents, $\lambda=400$ nm ($4.71\cdot10^{15}$ Hz, violet dotted line), $\lambda=509$ nm ($3.70\cdot10^{15}$ Hz, green dashed line), $\lambda=700$ nm ($2.69\cdot10^{15}$ Hz, red solid line): (e) Intensity profiles after linear diffraction. (f) Intensity profiles of the IWLLS. (g) Fourier, and (h) Floquet-Bloch power spectra of the IWLLS.

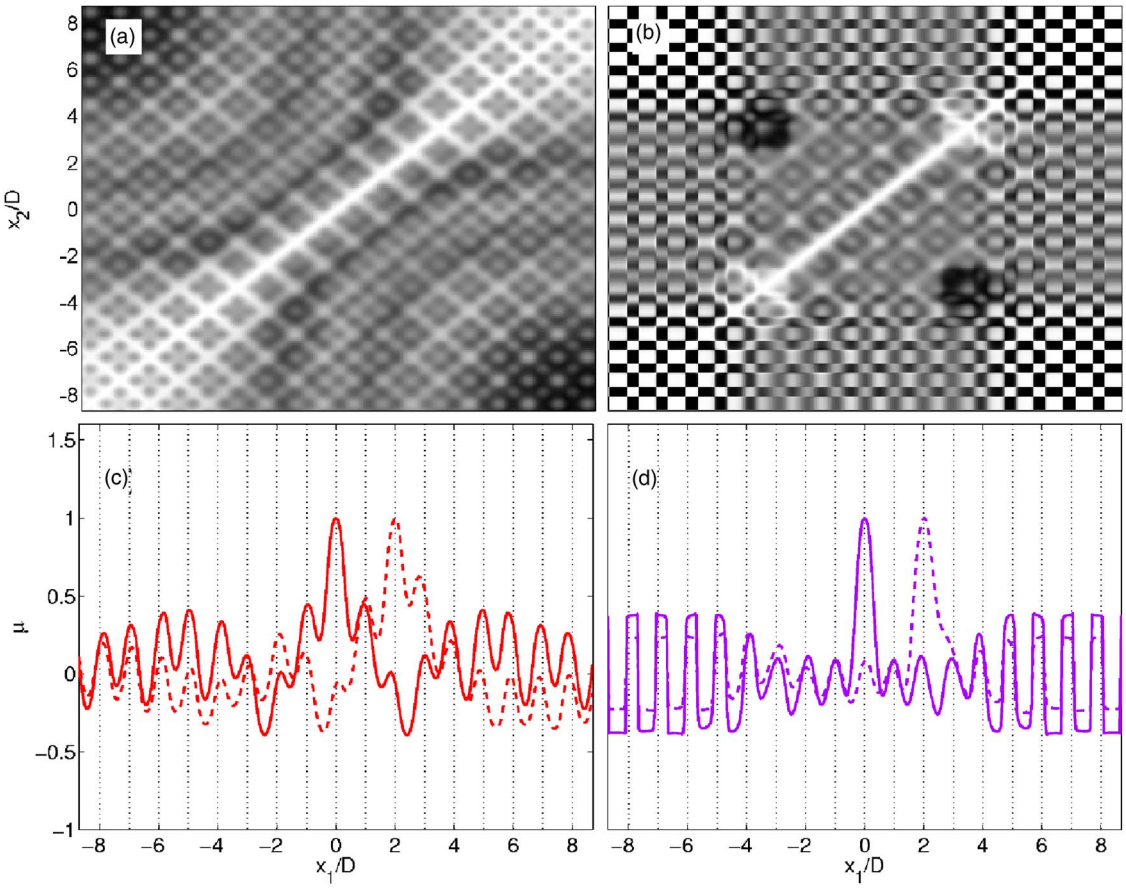

FIG. 3. (Color online) Contour plots of $\mu_\omega(x_1,x_2)$ expressing the coherence properties of the IWLLS at different frequency constituents. (a) $\mu_\omega(x_1,x_2)$ for the red constituent $\lambda=700$ nm, and (b) for the violet component $\lambda=400$ nm. Cross sections of the coherence factor, $\mu_\omega(x_1,0)$ (solid line), and $\mu_\omega(x_1,2D)$ (dotted line) for the red (c), and the violet (d) frequency constituent.

that in our calculations, we work in the parameter regime where the defect induced in the nonlinear medium by the IWLLS is smaller than the lattice depth, so that the basic lattice features are preserved in the presence of the soliton. Because different frequencies "feel" different effective lattices and nonlinearities, we conclude that in our example (of a "flat" temporal spectrum) it is harder to obtain soliton solutions that have a broader frequency range. (The fact that the spectral width of the incoherent white light can affect nonlinear phenomena was discussed previously in the context of modulation instability [38].) We test the stability of the calculated soliton numerically by evolving it (with small initial noise on top of the soliton modes) for many diffraction lengths.

The intensity structure and power spectra (see the Appendix for definitions) of the IWLLS example are plotted in Fig. 2, along with the linear diffraction behavior of the IWLLS launched in a linear lattice. Figure 2(a) shows the spatially oscillating intensity structure of the IWLLS. The humps in the intensity are located mainly on the lattice sites, which is consistent with the fact that 72% of the power is located in the localized modes originating from the first band [1,18]. When the lattice is linear, the initial profile diffracts instead of forming an IWLLS; Fig. 2(a) shows the beam properties after diffraction for $z=42$ mm. Figure 2(e) shows the intensity structure at three different wavelengths ($\lambda=400$, 509, and 700 nm) after linear diffraction. The largest wavelength experiences the strongest diffraction, because it evolves in lattice which is effectively most shallow. The intensity structure of different frequency constituents is shown in Fig. 2(f). Larger wavelength (smaller frequency) constituents have spatially broader profiles with smaller peaks at the lattice sites. This also follows from the fact that larger wavelengths experience a more shallow effective potential and a weaker nonlinearity. More pictorially, the intensity profile of the red part of the spectrum is wider, with smaller humps in the soliton region. The violet part of the spectrum shows the opposite behavior, with narrower intensity profiles and more pronounced humps in the soliton region (approximately, the height ratio resembles the frequency ratio).

The Fourier power spectra of the IWLLS are plotted in Figs. 2(c) and 2(g), while the Floquet-Bloch power spectra are plotted in Figs. 2(d) and 2(h). The total Fourier (Floquet-Bloch) power spectrum of the IWLLS is shown in Fig. 2(c) [Fig. 2(d), respectively] with solid line. Most of the spectrum is located in the normal diffraction regions, as the nonlinearity is of the self-focusing type [1–4]. Figure 2(g) [Fig. 2(h)] shows the Fourier (Floquet-Bloch, respectively) spatial power spectrum at different temporal frequency constituents. Within a single Brillouin zone, the spatial spectra corresponding to the smaller frequency constituents are more localized in k_x space. For example, the spectrum of the red

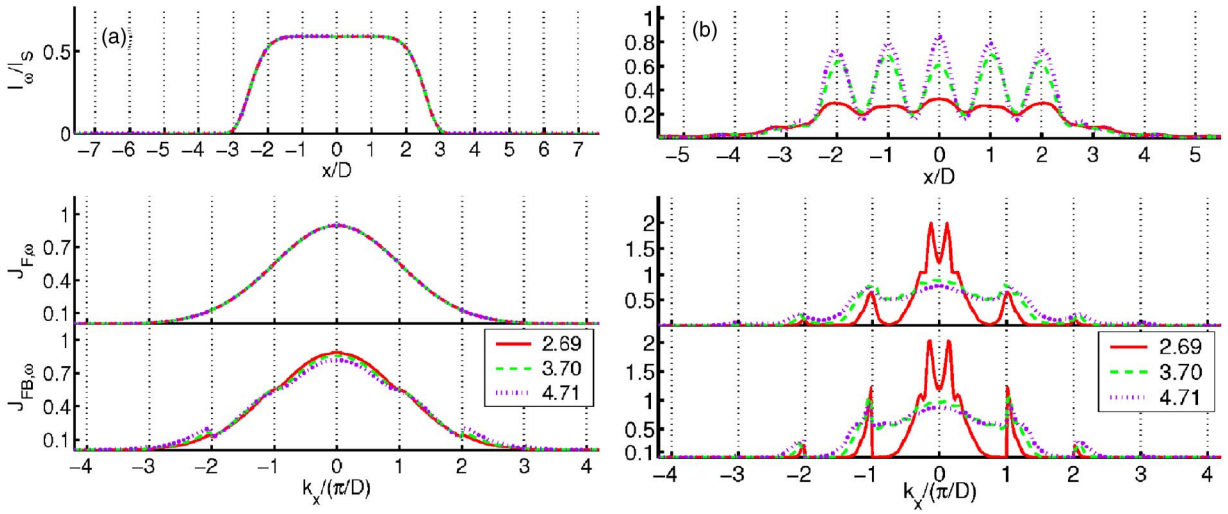

FIG. 4. (Color online) The intensity profiles, Fourier, and Floquet-Bloch spatial power spectra of a simple bell-shaped incoherent beam shown at different frequencies: $\lambda=400$ nm ($4.71\cdot10^{15}$ Hz, violet dotted line), $\lambda=509$ nm ($3.70\cdot10^{15}$ Hz, green dashed line), $\lambda=700$ nm ($2.69\cdot10^{15}$ Hz, red solid line). (a) The above quantities at the input $z=0$, and (b) after propagation for 42 mm. These properties at different frequency components differ from one another after propagation through the system.

component has very localized peaks within the first Brillouin zone for low k_x values [see solid line in Figs. 2(g) and 2(h)]. This is a consequence of the shallow effective lattice for the red component [see Fig. 1(a)].

Figure 3 illustrates the coherence properties of the IWLLS at different wavelengths. Coherence is expressed in terms of the complex coherence factor [Eq. (1)] at frequency ω, $\mu_\omega(x_1,x_2)$. The quantity $\mu_\omega(x_1,x_2)$ in Fig. 3 is real, in the range $[-1,1]$. The white (black) color in the contour plot denotes $\mu_\omega=1$ (-1, respectively), corresponding to coherence between the points x_1 and x_2. Gray corresponds to $\mu_\omega=0$, i.e., total incoherence. The coherence of an IWLLS at a given frequency mainly depends on the modal structure of the IWLLS at that frequency. In order to extract solely the dependence of the spatial coherence on the temporal frequency, in our IWLLS example, the excited modes and their weights are chosen to be identical at all frequencies. Figures 3(a) and 3(b) show $\mu_\omega(x_1,x_2)$ for the red and violet parts of the temporal spectrum. The red component has a (spatially) more extended modal structure, and therefore a broader area of smaller coherence (the grey region is broader for the red component). However, Figs. 3(c) and 3(d) illustrating the cross-sections $\mu_\omega(x_1,0)$ and $\mu_\omega(x_1,2D)$ for the red and the violet components, respectively, reveal that the red component is much more correlated from site to site than the violet (larger frequency) component. This also follows from the fact that larger frequency components have the same number of modes (with the same modal weights) squeezed within a smaller region of space, which yields a smaller coherence length at larger frequencies. The same feature holds for incoherent white-light solitons in homogeneous noninstantaneous nonlinear media [37].

IV. EVOLUTION OF AN INPUT INCOHERENT BEAM INTO A IWLLS

In this section we study the accessibility of incoherent white-light solitons in an experimental setting. In particular, we show that a "simple" incoherent white-light beam launched into the lattice can evolve, under proper nonlinear conditions, into an IWLLS. The parameters of the lattice and the nonlinearity are identical to the ones corresponding to the numerically exact soliton solution above. The modal structure of a simple, bell-shaped, input incoherent beam may be described by

$$\psi_{\omega;k_x}(x,z=0)=\sqrt{I^0(x)}G_\omega(k_x)e^{ik_x x}. \tag{7}$$

In our calculations the intensity structure of the beam is $I^0(x)=e^{-[x/(2.6D)]^8}$. Here, k_x is the transverse momentum of the k_xth mode $\psi_{\omega;k_x}$ at frequency ω. The continuous variable k_x here replaces the discrete index m. The function $G_\omega(k_x)\propto e^{-[k_xD/(2\pi)]^2}$ expresses the relative power within the $(\omega;k_x)$th mode. Note that we have chosen all frequency con-

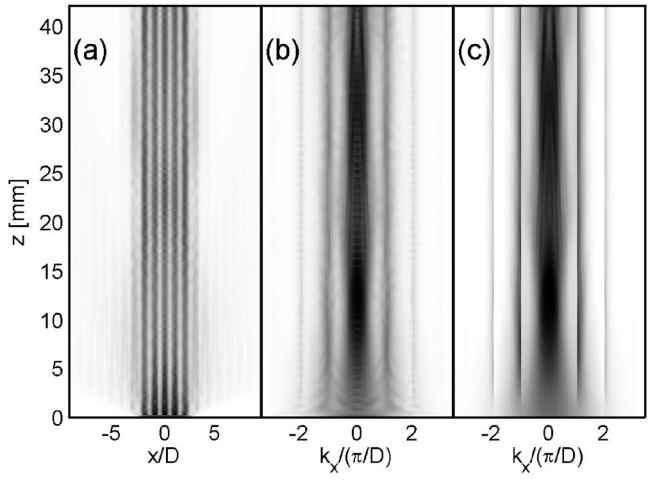

FIG. 5. The evolution of the total intensity profile (a), total Fourier power spectrum (b), and total Floquet-Bloch power spectrum (c) of an incoherent, bell-shaped, incoherent white-light beam launched into the nonlinear waveguide array (see text for details).

stituents to have the same intensity structure, Fourier power spectra, and coherence at the input [see Fig. 4].

Figure 5 shows the evolution of the intensity structure, the Fourier power spectrum, and the Floquet-Bloch power spectrum of the input beam. Shortly after the entrance into the lattice, the intensity profile of the beam becomes multihumped, conforming to the lattice structure. Similarly, the single humped power spectra (both Fourier and Floquet-Bloch) becomes multihumped, with humps mainly in the normal diffraction regions, due to the self-focusing nonlinearity [2,4]. We observe that after several diffraction lengths of propagation in the z direction, the beam reshapes itself into the solitonlike shape. Figure 4 shows the input and output intensity structure, spatial power spectra, and coherence of different frequency constituents. The beam is propagated for $z=42$ mm. Even though the input beam has the same shape for each frequency component, which clearly cannot be the case for an IWLLS, the beam naturally evolves into an IWLLS form (see Figs. 4). For example, the power spectra at the red component is narrower in k_x space at the output than other components, etc. We emphasize that this occurs solely due to the underlying dynamics, i.e., no specific engineering of the input beam was necessary. Figures 2(b)–2(d) show excellent matching of the self-adjusted beam, and the self-consistently calculated IWLLS. It is worth noting that the Floquet-Bloch power spectrum is obtained by using the appropriate basis for each frequency component, since this basis is itself frequency dependent. This can be seen in Fig. 4(a) (bottom inset), which shows the Floquet-Bloch power spectrum of the input beam at different wavelengths; even though the Fourier power spectrum is identical for all frequency components (at the input), the Floquet-Bloch power spectrum differs for different frequencies.

From Figs. 4 and 5 we find that the structure of the input incoherent beam evolves into the IWLLS structure obtained self-consistently. The evolution occurs via two mechanisms: (i) through a nonlinearity induced energy exchange between the Floquet-Bloch waves excited by the input beam (e.g., see Refs. [2,4] for discussion), and (ii) through a filtering effect to nonlocalized radiation (see Fig. 5); namely, some amount of power is radiated away from the localized beam during the initial process of self-adjustment of the input beam. It is interesting to note that during this process, longer wavelengths tend to be radiated more. This is natural to expect as they have a stronger tendency to diffract [e.g., see Fig. 2(e)]; thus, the temporal power spectrum is modified during the self-trapping process [this also depends on the spatial coherence properties at different wavelengths, which is in our case specified by the input beam structure, Eq. (7)]. After the beam becomes self-trapped, its properties do not change during further propagation, and its power is conserved.

V. CONCLUSION

In conclusion, we have theoretically studied incoherent white light lattice solitons in nonlinear waveguide arrays. We have examined the relevant physical properties of an IWLLS including the intensity structure, spatial power spectra, and coherence properties of different color constituents (from the visible spectral range $\lambda=400-700$ nm). The intensity profiles at lower temporal frequency constituents are broader, while the peaks in the intensity structure are lower. The opposite holds for the spatial power spectra at a given frequency: Spatial power spectra (Fourier and Floquet-Bloch) are narrower, with higher peaks at the lower frequency constituents (red part of the temporal spectrum). It is important to note that the aforementioned features of the IWLLS arise due to complex nonlinear coupling among the different color components: Each localized mode is formed by the self-consistent action of all other modes, including modes at different frequencies. We have also shown that such solitons are accessible experimentally in the sense that a simple incoherent white-light beam, when launched into the nonlinear lattice under suitable conditions, may naturally evolve into an IWLLS. We launched the same bell-shape profile for all wavelength components, and the nonlinear evolution process causes self-adjustment of the beam during the propagation, eventually resulting in a beam with the characteristic features of IWLLS, which are different at different frequencies.

The ideas of IWLLSs were presented here in the optical context. However, we believe that similar solitonic structures may be observed at finite temperature with multispecies Bose-Einstein condensates, where bosons from different species differ in their mass. The boson mass appears as a coefficient in the kinetic energy term of the many-body Schrödinger equation, in the same fashion as the wave-vector k_ω appears within the diffraction term of Eq. (3). This points towards further analogies between partially-coherent light in noninstantaneous nonlinear media and finite-temperature weakly- interacting Bose-Einstein condensates [43].

ACKNOWLEDGMENT

This research was supported by the Croatian Ministry of Science, and the Air Force Office of Scientific Research.

APPENDIX: DEFINITION OF POWER SPECTRA

For the clarity of the exposition, in this section we define the Fourier and Floquet-Bloch (FB) power spectra. When the periodic system is linear, the eigenmodes of the system are the FB modes $\phi_{\omega;nk_x}(x,z)=f_{\omega;nk_x}(x)e^{ik_x x+i\beta(\omega;k_x)z}$, obtained from the eigenvalue equation

$$\frac{1}{2k_\omega}\frac{d^2}{dx^2}[f_{\omega;nk_x}(x)e^{ik_x x}]+\frac{k_\omega}{n_0}p(x)f_{\omega;nk_x}(x)e^{ik_x x} = \beta(\omega;k_x)f_{\omega;nk_x}(x)e^{ik_x x}, \tag{A.1}$$

where $f_{\omega;nk_x}(x)=f_{\omega;nk_x}(x+D)$; n here denotes the band number, and k_x is the Bloch wave vector. The frequency dependent propagation constant of the Floquet-Bloch wave is $\beta(\omega;k_x)$, while the effective propagation constant of the FB mode is $2k_\omega x_0^2\beta(\omega;k_x)$. Note that the structure, and the propagation constants of the FB modes depend on the temporal frequency ω; e.g., the effective propagation constants of the FB waves as a function of frequency are plotted in

Fig. 1. The Floquet-Bloch power spectrum of the incoherent white-light beam at frequency ω is defined as

$$J_{\mathrm{FB},\omega}(k_x,z)=\sum_m d_{\omega,m}\left|\int dx\psi_{\omega;m}(x,z)f^{*}_{\omega;nk_x}(x)e^{-ik_x x}\right|^2. \quad \text{(A.2)}$$

We present the FB spectra in the extended-zone scheme. The Fourier power spectrum of the beam at frequency ω is defined as

$$J_{F,\omega}(k_x,z)=\sum_m d_{\omega,m}\left|\int dx\psi_{\omega;m}(x,z)e^{-ik_x x}\right|^2. \quad \text{(A.3)}$$

The total Floquet-Bloch $J_{\mathrm{FB,tot}}(k_x,z)$ and Fourier $J_{F,\mathrm{tot}}(k_x,z)$ power spectra are obtained by integration over all frequencies, that is, $J_{\mathrm{FB,tot}}(k_x,z)=\int d\omega J_{\mathrm{FB},\omega}(k_x,z)$, and $J_{\mathrm{FB,tot}}(k_x,z)=\int d\omega J_{FB,\omega}(k_x,z)$.

[1] H. Buljan, O. Cohen, J. W. Fleischer, T. Schwartz, M. Segev, Z. H. Musslimani, N. K. Efremidis, and D. N. Christodoulides, Phys. Rev. Lett. **92**, 223901 (2004).

[2] O. Cohen, G. Bartal, H. Buljan, J. W. Fleischer, T. Carmon, M. Segev, and D. N. Christodoulides, Nature (London) **433**, 500 (2005).

[3] G. Bartal, O. Cohen, H. Buljan, J. W. Fleischer, O. Manela, and M. Segev, Phys. Rev. Lett. **94**, 163902 (2005).

[4] H. Buljan, G. Bartal, O. Cohen, T. Schwartz, O. Manela, T. Carmon, M. Segev, J. W. Fleischer, and D. N. Christodoulides, Stud. Appl. Math. **115**, 173 (2005).

[5] K. Motzek, A. A. Sukhorukov, F. Kaiser, and Y. S. Kivshar, Opt. Express **13**, 2916 (2005).

[6] R. Pezer, H. Buljan, J. W. Fleischer, G. Bartal, O. Cohen, and M. Segev, Opt. Express **13**, 5013 (2005).

[7] G. Bartal, R. Pezer, H. Buljan, O. Cohen, O. Manela, J. W. Fleischer, and M. Segev, Opt. Lett. **31**, 483 (2006).

[8] D. N. Christodoulides, F. Lederer, and Y. Silberberg, Nature (London) **424**, 817 (2003).

[9] J. W. Fleischer, G. Bartal, O. Cohen, T. Schwartz, O. Manela, B. Freedman, M. Segev, H. Buljan, and N. K. Efremidis, Opt. Express **13**, 1780 (2005).

[10] D. N. Christodoulides and R. I. Joseph, Opt. Lett. **13**, 794 (1988).

[11] Yu. Kivshar, Opt. Lett. **18**, 1147 (1993); J. Feng, *ibid.* **20**, 1302 (1993).

[12] H. S. Eisenberg, Y. Silberberg, R. Morandotti, A. R. Boyd, and J. S. Aitchison, Phys. Rev. Lett. **81**, 3383 (1998).

[13] R. Morandotti, U. Peschel, J. S. Aitchison, H. S. Eisenberg, and Y. Silberberg, Phys. Rev. Lett. **83**, 4756 (1999); T. Pertsch, P. Dannberg, W. Elflein, A. Brauer, and F. Lederer, *ibid.* **83**, 4752 (1999).

[14] H. S. Eisenberg, Y. Silberberg, R. Morandotti, and J. S. Aitchison, Phys. Rev. Lett. **85**, 1863 (2000); T. Pertsch, T. Zentgraf, U. Peschel, A. Brauer, and F. Lederer, *ibid.* **88**, 093901 (2002).

[15] N. K. Efremidis, S. Sears, D. N. Christodoulides, J. W. Fleischer, and M. Segev, Phys. Rev. E **66**, 046602 (2002).

[16] J. W. Fleischer, T. Carmon, M. Segev, N. K. Efremidis, and D. N. Christodoulides, Phys. Rev. Lett. **90**, 023902 (2003).

[17] J. W. Fleischer, M. Segev, N. K. Efremidis, and D. N. Christodoulides, Nature (London) **422**, 147 (2003).

[18] O. Cohen, T. Schwartz, J. W. Fleischer, M. Segev, and D. N. Christodoulides, Phys. Rev. Lett. **91**, 113901 (2003).

[19] A. A. Sukhorukov and Y. S. Kivshar, Phys. Rev. Lett. **91**, 113902 (2003).

[20] D. Mandelik, H. S. Eisenberg, Y. Silberberg, R. Morandotti, and J. S. Aitchison, Phys. Rev. Lett. **90**, 053902 (2003).

[21] Y. Kartashov, V. Vysloukh, and L. Torner, Opt. Express **12**, 2831 (2004).

[22] J. Meier, G. I. Stegeman, D. N. Christodoulides, Y. Silberberg, R. Morandotti, H. Yang, G. Salamo, M. Sorel, and J. S. Aitchison, Phys. Rev. Lett. **92**, 163902 (2004).

[23] K. Motzek, A. A. Sukhorukov, Yu. S. Kivshar, and F. Kaiser, *Nonlinear Guided Waves and Their Application* (Dresden, Germany, 2005), p. WD25.

[24] M. Segev and D. N. Christodoulides, *Incoherent Solitons in Spatial Solitons*, edited by S. Trillo and W. Torruellas (Springer, Berlin, 2001) pp. 87–125.

[25] M. Mitchell, Z. Chen, M. Shih, and M. Segev, Phys. Rev. Lett. **77**, 490 (1996).

[26] M. Mitchell and M. Segev, Nature (London) **387**, 880 (1997).

[27] D. N. Christodoulides, T. H. Coskun, M. Mitchell, and M. Segev, Phys. Rev. Lett. **78**, 646 (1997).

[28] M. Mitchell, M. Segev, T. H. Coskun, and D. N. Christodoulides, Phys. Rev. Lett. **79**, 4990 (1997).

[29] V. V. Shkunov and D. Z. Anderson, Phys. Rev. Lett. **81**, 2683 (1998).

[30] D. N. Christodoulides, E. D. Eugenieva, T. H. Coskun, M. Segev, and M. Mitchell, Phys. Rev. E **63**, 035601(R) (2001).

[31] A. W. Snyder and D. J. Mitchell, Phys. Rev. Lett. **80**, 1422 (1998).

[32] B. Hall, M. Lisak, D. Anderson, R. Fedele, and V. E. Semenov, Phys. Rev. E **65**, 035602(R) (2002).

[33] M. Soljačić, M. Segev, T. Coskun, D. N. Christodoulides, and A. Vishwanath, Phys. Rev. Lett. **84**, 467 (2000).

[34] D. Kip, M. Soljačić, M. Segev, E. Eugenieva, and D. N. Christodoulides, Science **290**, 495 (2000).

[35] M. Peccianti and G. Assanto, Opt. Lett. **26**, 1791 (2001).

[36] A. Picozzi and M. Haelterman, Phys. Rev. Lett. **86**, 2010 (2001); A. Picozzi, M. Haelterman, S. Pitois, and G. Millot, *ibid.* **92**, 143906 (2004).

[37] H. Buljan, M. Segev, M. Soljačić, N. K. Efremidis, and D. N. Christodoulides, Opt. Lett. **28**, 1239 (2003); H. Buljan, A. Šiber, M. Soljačić, T. Schwartz, M. Segev, and D. N. Christodoulides, Phys. Rev. E **68**, 036607 (2003); H. Buljan, T. Schwartz, M. Segev, M. Soljačić, and D. N. Christodoulides, J. Opt. Soc. Am. B **21**, 397 (2004).

[38] H. Buljan, A. Šiber, M. Soljačić, and M. Segev, Phys. Rev. E **66**, 035601(R) (2002).

[39] T. Schwartz, T. Carmon, H. Buljan, and M. Segev, Phys. Rev. Lett. **93**, 223901 (2004).
[40] S. A. Ponomarenko, N. M. Litchinitser, and G. P. Agrawal, Phys. Rev. E **70**, 015603(R) (2004).
[41] M. Shen, Q. Wang, J. Shi, Y. Chen, and X. Wang, Phys. Rev. E **72**, 026604 (2005).
[42] O. Cohen, H. Buljan, T. Schwartz, J. W. Fleischer, and M. Segev, Phys. Rev. E **73**, 015601(R) (2006).
[43] H. Buljan, M. Segev, and A. Vardi, Phys. Rev. Lett. **95**, 180401 (2005).